Coupling tree-ring and geomorphic analyses to reconstruct the 1950s massive Glacier Lake Outburst Flood at Grosse Glacier, Chilean Patagonia

S. Gorsic [a,*], C. Corona [a,b], A. Muñoz-Torrero Manchado [a,c], J. Lopez-Saez [a], S. Allen [a,d], J.A. Ballesteros-Cánovas [a,c], A. Dussaillant [e,f,g], M. Stoffel [a,h,i]

[a] Climate Change Impacts and Risks in the Anthropocene (C-CIA), Institute for Environmental Sciences, University of Geneva, Geneva, Switzerland
[b] Université Grenoble Alpes, CNRS LECA, Grenoble, France
[c] National Museum of Natural Sciences, MNCN-CSIC, C/Serrano 115bis, 28006 Madrid, Spain
[d] Department of Geography, University of Zürich, Zürich, Switzerland
[e] Centro de Investigaciones en Ecosistemas de la Patagonia, Coyhaique, Chile
[f] Universidad de Aysén, Coyhaique, Chile
[g] UK Centre for Ecology & Hydrology, Wallingford, United Kingdom
[h] dendrolab.ch, Department of Earth Sciences, University of Geneva, Geneva, Switzerland
[i] Department F.-A. Forel for Environmental and Aquatic Sciences, University of Geneva, Switzerland

HIGHLIGHTS

- Multi-proxy approach allows dating of massive Grosse Glacier GLOF to October 1957.
- Object-based image analysis and dendrogeomorphology help map extent of GLOF.
- More reconstructions are needed in secluded areas to complement GLOF inventories.
- In addition to the 1957 GLOF, tree-ring analysis allows reconstructing five smaller floods.

GRAPHICAL ABSTRACT
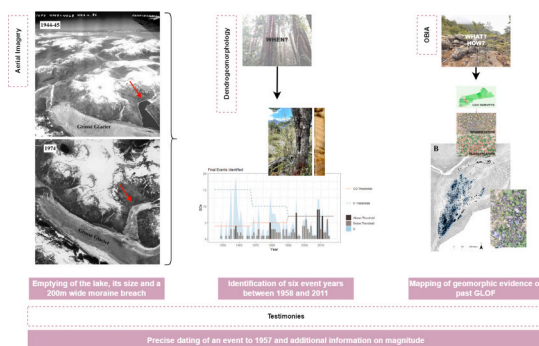
ARTICLE INFO

ABSTRACT

Over recent decades, global warming has led to sustained glacier mass reduction and the formation of glacier lakes dammed by potentially unstable moraines. When such dams break, devastating Glacial Lake Outburst Floods (GLOFs) can occur in high mountain environments with catastrophic effects on populations and infrastructure. To understand the occurrence of GLOFs in space and time, build frequency-magnitude relationships for disaster risk reduction or identify regional links between GLOF frequency and climate warming, comprehensive databases are critically needed. GLOF inventories have thus been compiled at both regional and global scales. While these accounts offer valuable data for hazard assessment, many GLOF events are omitted because they occurred before the satellite era or prior to the installation of river gauges, went unreported or were only mentioned in local media but not documented in the scientific literature. In addition, while geomorphic evidence

* Corresponding author.
  E-mail address: sandra.belin-gorsic@unige.ch (S. Gorsic).

of past GLOFs exist, their timing oftentimes remains unknown. These discontinuities preclude the identification of return periods for the most disastrous events and makes the link between GLOFs and ongoing climate warming remain inconclusive. To overcome these limitations, long-term records have been developed using a wide variety of proxies. Here, we explore the potential of coupling dendrogeomorphology and geomorphic analyses to reconstruct a GLOF event that occurred before the satellite era. The Grosse Glacier outlet, in San Rafael National Park, Chilean Patagonia, was selected based on satellite imagery, historical photographs and local testimonies indicating a previous lake drainage. Tree-ring analysis allowed identification of a massive GLOF and five smaller floods from 105 disturbed *Nothofagus* and *Podocarpus* trees. Unmanned aerial vehicle (UAV) imagery and object-based image analysis (OBIA) were used to identify boulders and to estimate flow direction in the glacio-fluvial floodplain and point to the occurrence of at least one high-energy flow event. Aerial photo analysis also revealed the formation of a 200-m-wide breach in the frontal moraine and the disappearance of a lateral lake, estimated to be 1.8 km² in size, sometimes after 1944–45. An in-depth interview with an eyewitness pinpointed the date of the GLOF to October 1957, in line with the estimated date of damage in the tree-ring records and precipitation records at Puerto Aysén. When used in conjunction, the different approaches contribute valuable insights into the timing and consequences of past extreme events, thus aiding in future assessments of GLOF hazards, not only at the Grosse Glacier but also in other high-mountain environments.

1. Introduction

With the Intergovernmental Panel on Climate Change (IPCC) projecting an alarming 18–36 % reduction in glacier mass by the end of this century, significant geomorphic and hydrological changes are anticipated to unfold in glaciated environments (IPCC, 2021; Hock et al., 2019). Due to these changes in the cryosphere, peri- and para-glacial lakes formed following glacier retreat and dammed by unstable moraines have been rapidly increasing in number and total area globally between 1990 and 2018 (Shugar et al., 2020). This trend has led to predictions that, with continued climate warming and glacier mass loss, the source location, seasonality, frequency and magnitude of glacial lake outburst floods (GLOF) – defined as the sudden release of water from bedrock-, ice- or moraine-dammed lakes in glacial environments (Clague, 2000; O'Connor and Costa, 1993) – will increase, along with the associated hazards (IPCC, 2021; Taylor et al., 2023). As they are often characterized by extreme flood volumes and peak discharges, their possible occurrence thus is of increasing concern to communities and infrastructure, sometimes located tens to hundreds of kilometers downstream of critical lakes (Harrison et al., 2018; Stuart-Smith et al., 2021; Emmer et al., 2022; Cenderelli and Wohl, 2003; Jacquet et al., 2017; Cook et al., 2018).

GLOF inventories have been compiled at both regional (Harrison et al., 2018; Emmer et al., 2022; Colavitto et al., 2024) and global (Veh et al., 2022) scales using various sources, including documentary and monitoring records, grey literature, field surveys and satellite image analysis. Whereas GLOF inventories are rather complete for the recent past, records become much more lacunary as soon as they extend beyond the satellite era or gauged river-flow datasets. These potential biases makes it unclear whether the apparent increase in reported GLOF occurrences is linked to a warming atmosphere or to a growing research attention with access to increasingly detailed data coverage (Veh et al., 2022; Rick et al., 2023). One avenue for reducing such biases is the construction of historical GLOF databases with dendrogeomorphic techniques (Stoffel and Bollschweiler, 2008; Stoffel and Corona, 2014). Such approaches have proven to substantially improve the baseline knowledge of hazard processes, yield precise occurrence dates and particularly frequency–magnitude relations in mountain regions (Zaginaev et al., 2016; Zaginaev et al., 2019; Stoffel et al., 2011; Ballesteros-Cánovas et al., 2020).

In this study, we explore the potential of two methods, dendrogeomorphology and UAV-based geomorphic analyses, to extend GLOF reconstruction beyond the period covered by satellite images in a remote region where detailed documentation is generally lacking and diagnostic features potentially rapidly vanish due to vegetation succession and geomorphic reworking (Emmer, 2023). Specifically, we focus on characterizing a GLOF that occurred sometimes after 1944–45, likely following the disappearance of an ice-dammed lateral lake on the

southwestern flank of Grosse Glacier, located in the San Rafael National Park (Chilean Patagonia) near the North Patagonian Icefield (NPI). To do so, we employ growth disturbances in tree-ring series to identify potential dates of the GLOF. In addition, we rely on unmanned aerial vehicle (UAV) imagery acquired during fieldwork to combine geomorphic analyses with object-based image analysis (OBIA) to identify boulders and deposits left by the GLOF and to estimate flow direction. The findings are then contrasted with an eyewitness account from an elderly resident who apparently witnessed the GLOF.

2. Study area

2.1. GLOFs in the Northern Patagonian Icefield region

Ice-dammed lakes are particularly common in the NPI, forming behind glaciers that advanced during the Little Ice Age (LIA) (Blaschke et al., 2014). As a result of glacier melting, the area of these glacial lakes has increased by 65 % between 1945 and 2016 in the region. In addition, and as these glacier retreat and thin (Loriaux and Casassa, 2013a), the potential for outburst-floods increases (Jacquet et al., 2017; Vandekerkhove et al., 2021; Veh et al., 2023; Dussaillant et al., 2019; Dussaillant et al., 2010; Benito et al., 2021), with potential for cascading process chains when subsequent downstream lakes are impacted and large sediment volumes mobilized (Mani et al., 2023).

Existing databases of past GLOF occurrences in the Andes have been compiled using satellite imagery (Veh et al., 2022), and were complemented with field surveys, and documentary data sources (Emmer, 2017). These databases show a clear increasing trend in GLOF frequency since the 1970s due to more consistent GLOF reporting and increasing availability of satellite imagery (Emmer et al., 2022; Veh et al., 2022). In contrast to the Peruvian and Bolivian Andes, GLOF dynamics across Chile and Argentina, and in particular in the NPI, the largest body of non-polar ice worldwide, remain poorly documented (Burton et al., 2022). This is particularly noteworthy as glaciers there shrink two times faster between 2001 and 2011 than during the 1870–1986 period (Davies and Glasser, 2012), and as evidence for multiple GLOF occurrences in this region pose an increasingly hazardous challenge to urbanization, which rapidly expands into formerly isolated areas (Burton et al., 2022), and to tourism which develops rapidly in the San Rafael National Park. The global GLOF inventory for the Patagonian Andes contains 160 historic events, mostly around NPI and the Southern Patagonian Icefields (Veh et al., 2022). Colavitto et al. (Ref. (Colavitto et al., 2024) recently added 35 previously unknown GLOFs to this database, bringing the total number of documented GLOFs to 195. Of these, the exact year of occurrence is only known for 69 events.

In the immediate vicinity of our study site, the Grosse Glacier, documented events just include a 2015 GLOF from a moraine dammed lake in the Chileno Valley entering into an ice-dammed lake located on

the eastern flank of ExplorADores Glacier (Wilson et al., 2019), and a GLOF from another ice-dammed tributary of the Exploradores Glacier in 2018 (Veh et al., 2022).

2.2. The Grosse Glacier

The Grosse Glacier (46°26′27 S - 73°17′22 W) is a temperate glacier situated at the north-eastern extremity of the NPI in Chile (Fig. 1). Encompassing a total area of approximately 78 km², its equilibrium line is situated at low altitude (1096 m asl) compared to other glaciers from the icefield (Rivera et al., 2007). While the extent of the Grosse Glacier remains largely unknown for the first half of the 20th century, ice retreat was very slow between 1970 and 1991 because the glacier was almost entirely covered by thick debris from shear walls on the north face of Monte San Valentin. Considerable retreat (c. 1400 m) was, by contrast, reported between 2002 and 2004 and can likely be attributed to snout disintegration (Aniya, 2017a). Until 2007, snout retreat slowed down to c. 50 m yr⁻¹ before it increased again to c. 250 m yr⁻¹ (2007–2008). Between 2008 and 2012, the glacier stagnated before a slow retreat was again documented until 2015 with 50 m yr⁻¹. In front of the Grosse Glacier, a proglacial lake started to appear in c. 1986 and progressively enlarged by coalescing with supraglacial ponds (Aniya, 2017a; Loriaux and Casassa, 2013b); the lake is dammed by a 70-m high frontal moraine, probably from the Little Ice Age (Mardones et al., 2018).

The studied fluvioglacial plain lies 100 m below the glacier's frontal moraine and consists of several discharge channels. The central part of the plain is covered by multiple boulders and deposits as well as remnants of older moraines (Mardones et al., 2018). The area is colonized by a mature forest stand composed of evergreen and deciduous *Nothofagus* species as well as *Podocarpus nubigenus*, an evergreen conifer). Moreover, a paved tourist road (X-728) crosses the site on its way from the town of Puerto Rio Tranquilo to the *Exploradores* river delta (Fig. 1).

Aerial photographs from 1944 to 45 show the presence of an ice-dammed lateral lake on the southwestern flank of the glacier (Fig. 2). In the 1974 photograph, the lake is shown as empty, revealing a 200-m-wide breach in the moraine, two distinct river discharge channels, and a large area where vegetation has disappeared (Fig. 2). By coupling the ALOS PALSAR digital elevation model (DEM; 12.5 m pixel⁻¹) with the historical water level line georeferenced from the digitized 1944–45 aerial photo, we estimate the lake volume at 45×10^6 m³ with an area of 180 ha. As a result of the assumed GLOF, the morphology of the fluvioglacial plain was strongly modified: the main channel of the pro-glacial river was pushed northwards, presumably as a result of substantial sediment accumulation (Fig. 2). This sediment likely originated from the moraine breach at the southern part, where the secondary discharge channel is located. Likewise, the forest mainly vanished from the fluvioglacial plain between 1944 and 45 and 1974, except for a preserved sector in the central southern part where the stand persisted, although it was likely affected by the flood too.

The proximity of the NPI to the ocean and the southern latitude – prone to westerly winds – explain the frequent and abundant precipitation at the site (Aniya, 2013) totaling an estimated 6000–7000 mm per year (Aniya, 2017b). Such consequent precipitation amounts provide the necessary basis for glaciers to accumulate at low altitudes. The 0 °C isotherm in the study region was calculated to be around 2000 m asl in summer and 900 m asl in winter, with an equilibrium line of the glacier
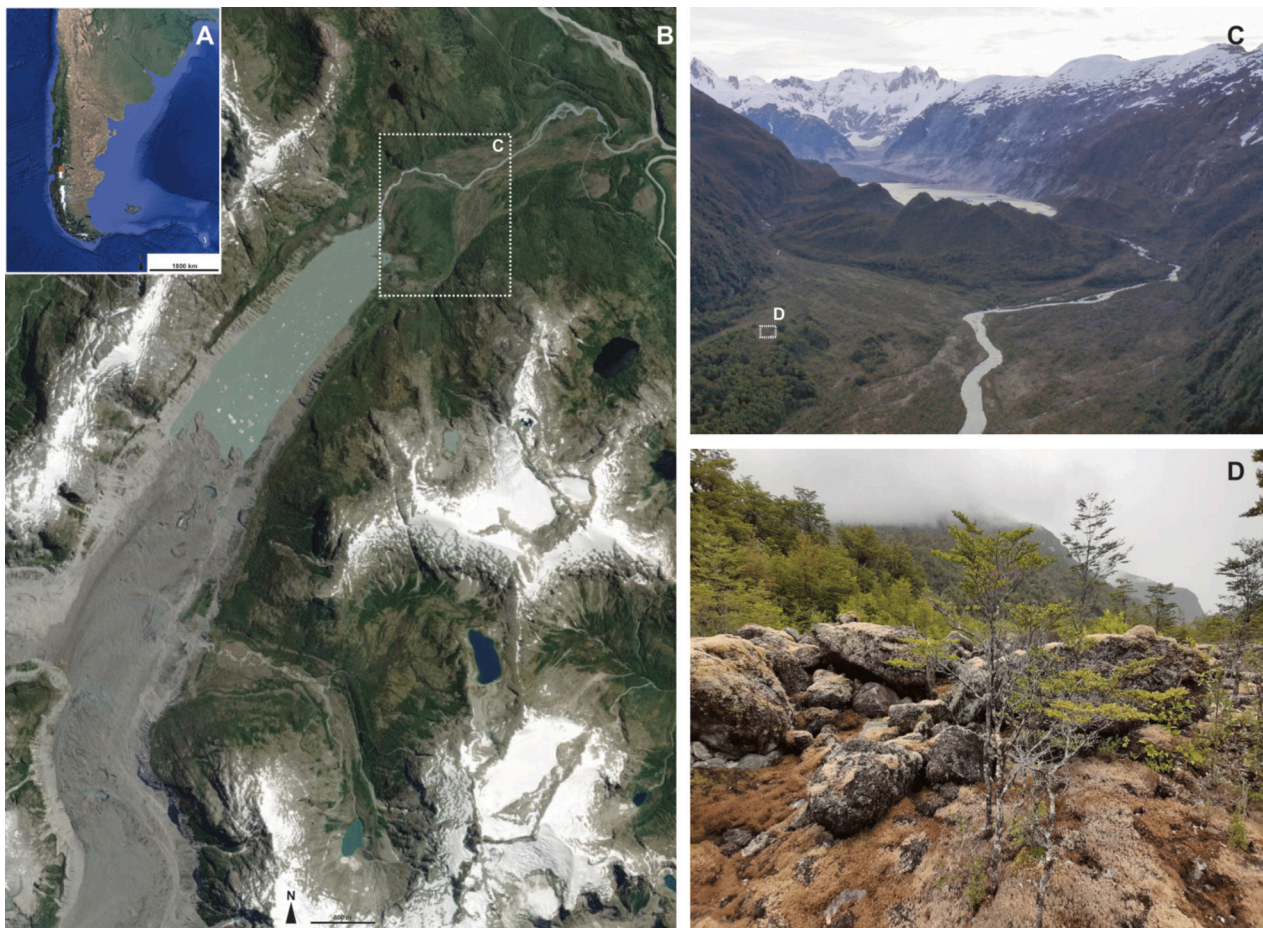

Fig. 1. The study site is at the outlet of the Grosse Glacier, situated in the Laguna San Rafael National Park (B). Aerial picture showing the frontal moraine damming the proglacial lake of Grosse Glacier (C) and the fluvioglacial plain where numerous boulder deposits can be found; this is also where the dendrogeomorphic sampling was conducted (D).
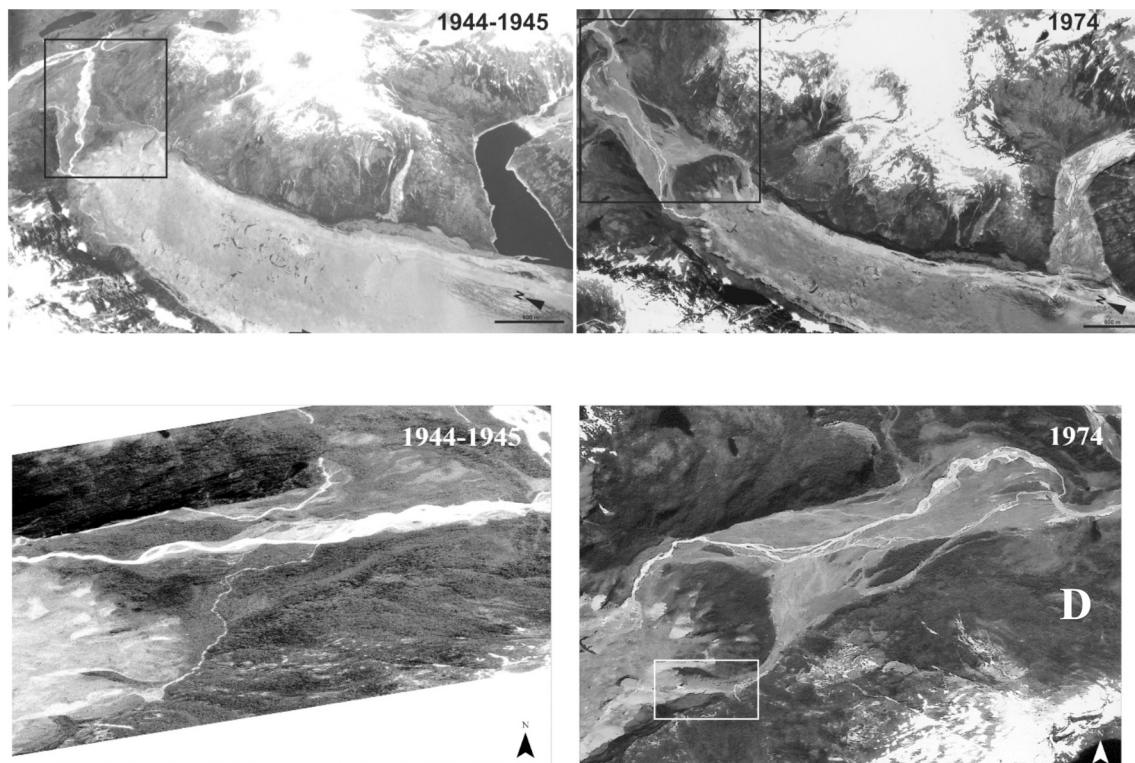
Fig. 2. Evolution of Grosse Glacier and surroundings between 1944 and 45 (left panels) and 1974 (right panels). Comparison of large-scale photographs clearly shows the presence of a lateral lake in 1944–1945, which had disappeared by 1974. Details of the aerial photographs (rotated by 120° to focus on the moraine and the fluvio-glacial plain) evidence a moraine breach (right – lower panel) subsequent to the purge. Black squares (upper panel) delineate the fluvio-glacial plain where analysis was conducted. The photographs were taken by the United States Military Service flight using a trimetrogon camera.

at ~1000 m asl (Willis et al., 2012).

Records from the nearest meteorological station (Puerto Aysén), located some 120 km from the Grosse Glacier, show a marked increase in winter precipitation at the end of the 1920s, followed by warmer and drier conditions between 1938 and 1948 as well as important decadal fluctuations in spring and winter temperatures until 1972 (Mardones et al., 2018). Notably, between 1944 and 1974, i.e. the time window during which the ice-dammed lateral lake disappeared, we find two particularly rainy winters in 1958 and 1971 (Mardones et al., 2018). It remains, however, uncertain to what degree these temperature and precipitation anomalies may have contributed to the GLOF at Grosse Glacier.

3. Material and methods

To document and possibly date the GLOF at this particular site of the NPI region, we developed an original multi-disciplinary approach. This approach combines (1) growth-ring analyses of trees presumably damaged by the GLOF to possible date the event as well as (2) photogrammetric and object-based image analyses (OBIA) of high-resolution aerial photographs to validate the occurrence of the event and precisely delineate its spatial extent. Results from this approach are ultimately validated against eye-witnesses accounts, and people's experiences provide data about the timing, extension, and damage induced by the flood.

3.1. Dating the GLOF with flood-damaged trees

The forest stand covering the fluvio-glacial plain of the Grosse Glacier, downstream of the glacial lake, hosts many trees with obvious signs of an extreme flood that visibly occurred many decades ago and therefore offers the opportunity to study these heavily damaged trees with dendrogeomorphic approaches (Stoffel and Corona, 2014) (Fig. 3A-

E). Dendrogeomorphology, the study of trees affected by past geomorphic process activity, is in fact based on the identification and the dating of growth disturbances (GDs) in tree-ring series has been used repeatedly over the last decades to reconstruct past floods and debris flows worldwide (Bollschweiler and Stoffel, 2010; Šilhán, 2023) at local and regional scales (Šilhán, 2023; Stoffel et al., 2014; Schraml et al., 2015; Franco-Ramos et al., 2019; Tichavský et al., 2022). With the exception of a study in the Tien Shan Mountains of Kyrgyzstan (Zaginaev et al., 2016), where the authors differentiated GLOFs from debris flows based on the spatial distribution (or umbrella) of damaged trees and the runout distances of events, dendrogeomorphic approaches have not hitherto been applied to understand past GLOF activity.

3.1.1. Sampling strategy

We used high-resolution images from the ESRI World Imagery database available in ArcGIS Pro, i.e. Landsat 4–5 TM, 7 ETM and 8 OLI (1985-now), Sentinel 2 A and Sentinel 2B (2015-now) satellite imagery to identify potential discharge channels and changes thereof at the outlet of Grosse Glacier. In addition, we complemented analyses with the 1944–45 and 1974 aerial photographs from United States Military Service Flights (Trimetrogron camera). Based on the results of this photointerpretation, we identified areas of interest (Fig. 3) for dendrogeomorphic sampling. A dendrogeomorphic sampling of 105 trees was realized in November 2019 and relied on the species available at the study site, i.e. *Nothofagus dombeyi (n = 88), Nothofagus pumilio (n = 9)* and *Podocarpus nubigenus (n = 8)* (Fig. 3B). The nature of damage identified in these trees was mostly in the form of scars visible on the stem surface; often-at considerable heights above ground. These scars were interpreted in the field to reflect the impact of rolling boulders or floating trees transported by an unusual flood impacting trees. In addition to scarred trees, we also sampled trees with signs of decapitation or burial (Stoffel and Bollschweiler, 2008). Dendrogeomorphic sampling (Stoffel and Corona, 2014) consisted of the extraction of two increment
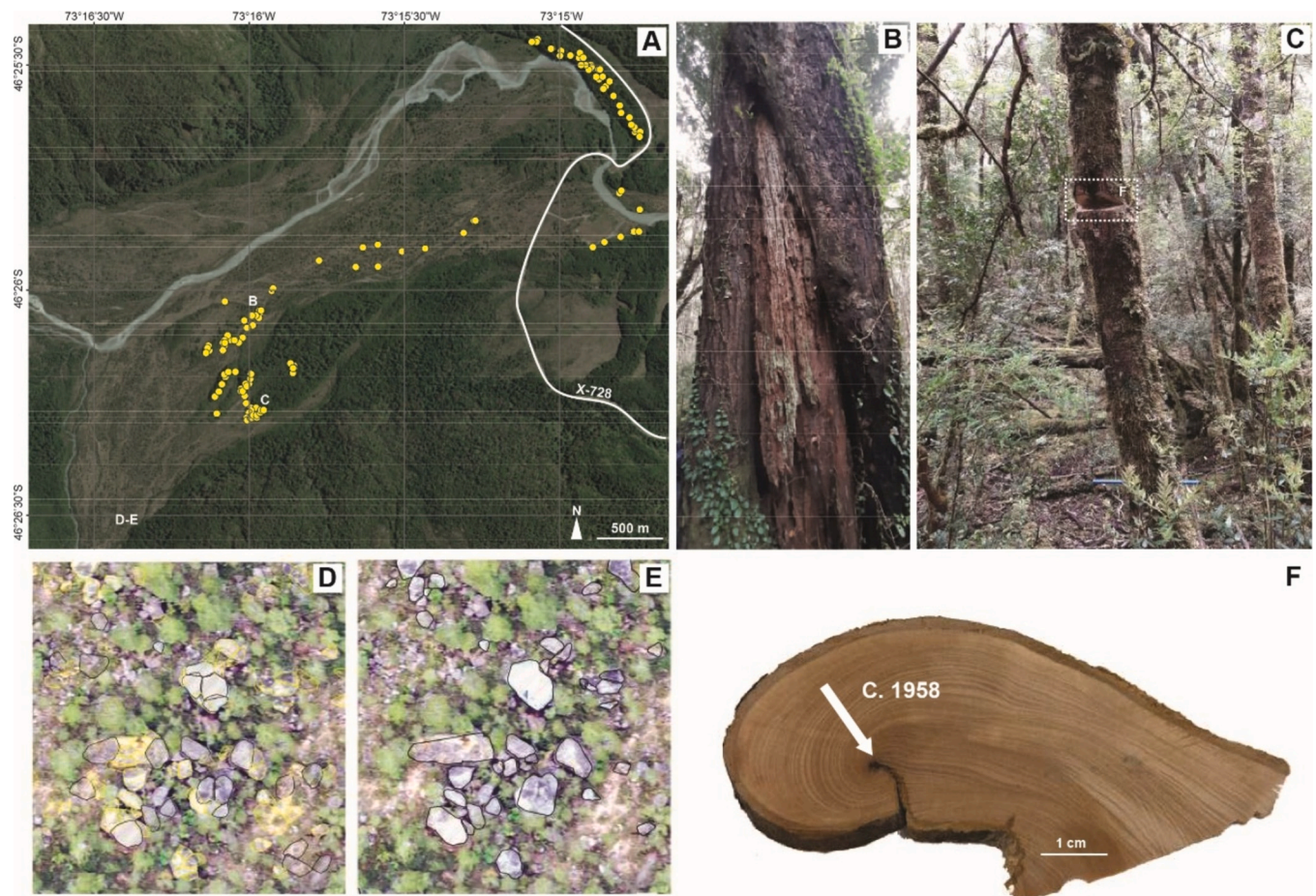
Fig. 3. The fluvio-glacial plain (A) with the sampled trees (yellow dots) and road X-728 from the town of Puerto Rio Tranquilo to the Exploradores river delta (white line). A total of 105 trees with clear signs of GLOF or flood damage in the form of scars (B) or apex decapitation with scars (C) were sampled in the field, either by extracting increment, wedges (F) or cross-sections. The arrow in panel F points to a scar that we dated to *c.* 1958. Relying on an object-based image analysis (OBIA), we mapped individual boulders and larger deposits on highly-resolved UAV images (D, E).

cores (Ø 5.5 mm) per tree. Sampling of scars was limited to trees for which the position of damage was in the assumed flow direction of the GLOF. Consequently, we avoided trees with scars pointing to lateral slopes to eliminate potential damage from rockfall. Samples from wounded trees were taken at the contact between the scar and the intact wood to make sure that the entire tree-ring record was available on the core (Stoffel and Corona, 2014; Zaginaev et al., 2016; Ballesteros et al., 2010). Although a large majority of the sampling was carried out with increment borers, wedges ($n = 9$) and cross sections ($n = 18$) were taken occasionally with a handsaw. Tree coordinates were obtained with an accuracy <1 m with a Trimble GeoExplorer GPS. For each tree, additional data were collected including its position within the floodplain, its diameter at breast height (DBH), description of the disturbance (i.e., impact scars, branch flagging, stem burial and decapitation, relative orientation of damage to the flow) and information on neighboring trees.

3.1.2. Tree-ring analysis

Samples were analyzed and data processed following standard dendrochronological procedures (Stoffel and Bollschweiler, 2008; Bräker, 2002). Single steps of surface analysis included sample mounting on a slotted mount, drying, and surface preparation by fine sanding the upper core surface up to grit size of 600 that allowed the annual rings to be easily recognized under magnification. We carefully counted tree-rings and measured ring widths from high-resolution (1200 dpi), digitized images using the CooRecorder 9.0 software (Larsson, 2013). We then inspected each sample to detect GDs resulting from the

mechanical impact of debris and floating stems such as chaotic callus tissue and/or abrupt reductions in trees. A marked reduction in annual ring widths was noted if it persisted for at least five consecutive years and if the width of the first narrow ring was 50 % or less of the width of the annual ring of the previous year (Stoffel and Bollschweiler, 2008; Stoffel and Corona, 2014). Such growth reductions generally reflect damage to the root system, loss of a major limb, or partial burial of the trunk by sediments (Bollschweiler et al., 2007; LaMarche, 1968). Northern Patagonia's growing season starts in October and ends in March (Suarez, 2010; Masiokas and Villalba, 2004), this is why for the sake of clarity we dated GDs to the year in which ring growth started (i.e. 2018 for the 2018/2019 season), as suggested by Schulman (Schulman, 1956) and usually used as a reference in numerous articles (Suarez, 2010).

3.1.3. Detection of past events in tree-ring series

Determination of events was based both on the number of samples showing GDs in the same year and the spatial distribution of affected stems (Bollschweiler et al., 2008). Data from individual trees was then summarized in event response histograms (Shroder, 1978; Dubé et al., 2004; Reardon et al., 2008). For each year t, an index I was calculated based on the percentage of trees showing responses in their tree-ring record in relation to the number of trees sampled being alive in year t:

$$\mathrm{It} = \left(\left(\sum_{i=1}^{n} \mathrm{Rt} \right) \Big/ \left(\sum_{i=1}^{n} \mathrm{At} \right) \right) \times 100$$

To take changes in sample depth (i.e. the number of trees available for analysis in any given year) into account, we discriminated events from not-event year relying on varying *It* and *GD* thresholds: that is, for instance, for a sample size of 10–20 trees, we considered that an event occurred if the number of GD was≥3 and the It ≥15 %. This definition of optimal values for GD and *It* has been defined at sites for which damage in trees and the resulting reconstruction of geomorphic process activity could be cross-validated against historical records, with the aim to (i) maximize the match between documented and reconstructed events while (ii) minimizing possible noise inherent to tree-ring records (Corona et al., 2012; Morel et al., 2023; Stoffel et al., 2017). In a final step, the spatial distribution of damaged trees was used to validate our reconstruction (Schneuwly-Bollschweiler et al., 2013).

3.2. Mapping the flow direction of the GLOF using object-based analysis

3.2.1. Boulder accumulations as markers of past GLOF events

GLOFs suddenly release large volumes of impounded water into the fluvial network (Ruiz-Villanueva et al., 2017) and can have large impacts on the morphology of downstream valleys. They induce strong erosion in some places and the deposition of huge amounts of sediment in other locations, including large boulders (Cenderelli and Wohl, 2003; Costa, 1983; Kershaw et al., 2005) that otherwise remain stationary even during intense rainfall-driven floods (Cook et al., 2018; Huber et al., 2020; Dahlquist and West, 2022). GLOF signs can thus potentially be preserved in the landscape several decades or centuries after an event (Baker, 2002; Rudoy, 2002). In particular, clusters of far-traveled boulders are considered as a proxy for the reconstruction of past "superfloods" (Baker, 2002) with high energy. Characteristics of such high-magnitude deposits can thus be used to differentiate floods from GLOFs. Post-event observations suggest that debris flow fronts, laden with large boulders when reaching flat sectors, tend to become deposited when losing the confinement of the upstream channel (Coussot and Meunier, 1996; Piton et al., 2018; Piton et al., 2022). Such boulder accumulations in flat sectors are thus considered to be the most reliable markers of past GLOFs (Lambiel et al., 2020). Additionally, elongated pebbles and boulders typically align parallel to the flow, with their longest axes oriented in the direction of deposits in high-energy, lower-density flows. In contrast, lobes align perpendicular to the flow due to the abrupt loss of energy and density, coupled with increased basal and lateral friction forces (Karatson et al., 2002; Bertran et al., 1997; Major, 1998; Iverson et al., 2010; Brenna et al., 2020; Kohlbeck et al., 1994; Rust, 1972). In the field, we identified several in-situ deposits and a perpendicular arrangement of boulders along their fronts. Therefore, we precisely characterized boulder deposits in the fluvio-glacial plain with OBIA and used the accumulation patterns and boulder orientations as potential indicators of the GLOF event. The steps of the process used to detect the deposit and the boulder as well as map their orientation on the fluvio-glacial plain are detailed in Fig. 4.

3.2.2. High resolution aerial images from UAV and photogrammetric processing

Unlike satellite-based sensors or aerial imagery, unmanned Aerial Vehicle (UAV) photogrammetry can provide high-resolution images with centimetric resolution and thus allows generations high-resolution topographic data (Digital Elevation Models, DEMs) and orthophotos of exceptional detail and resolution (Fang et al., 2021), making it possible to calculate various morphometric attributes (Fiolleau et al., 2022). High-resolution images of the frontal moraine and the fluvioglacial plain, covering an area of 7.8 km^2, were acquired with DJI Mavic 2 Pro and Ebee Classic drones in November 2019. We performed a total of 12 UAV flights at altitudes ranging from 200 to 500 m above the ground, and cameras oriented at 75° to better capture steep terrains such as the frontal moraine walls (Fig. 4, step 1).

Each UAV flight incorporated a double grid mission strategy, capturing images along two primary perpendicular directions. This
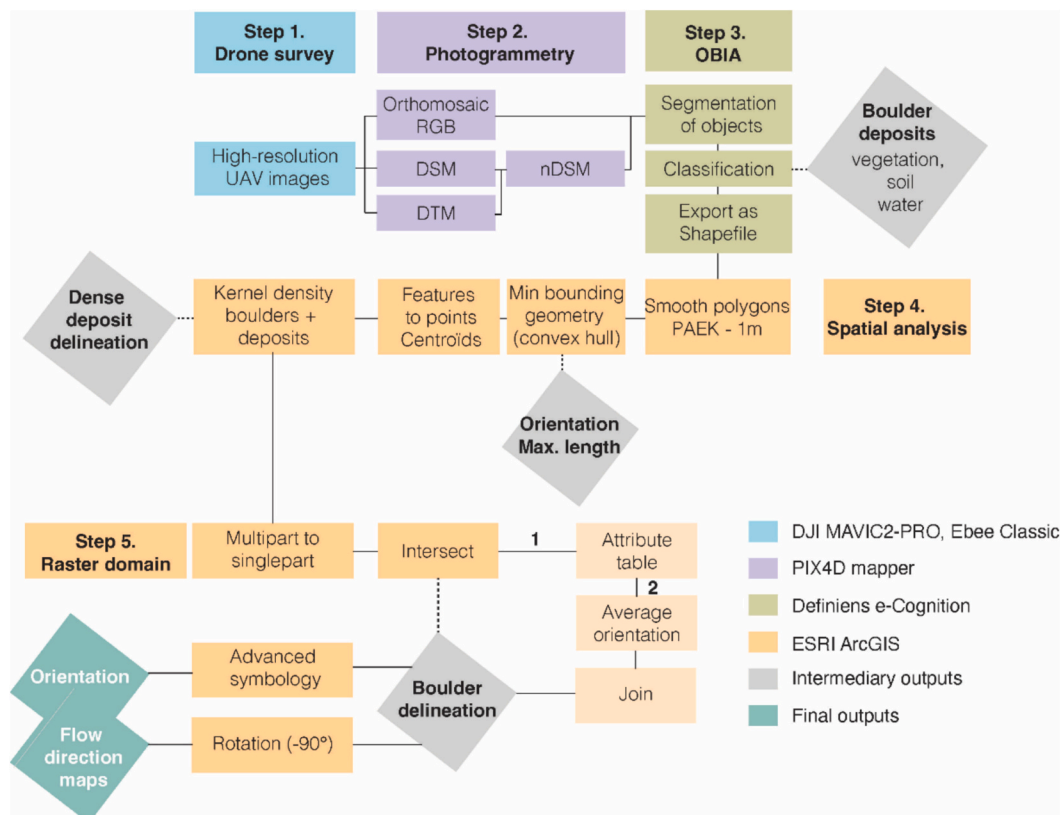

Fig. 4. Detailed overview of the procedure used to derive boulder orientation and flow direction maps from UAV-derived aerial photographs.

approach was chosen to enhance the accuracy and quality of 3D models, particularly in steep and complex terrain. Acquisition resolutions varied from 4.85 (200 m) to 12.12 cm pixel^{-1} (500 m). A minimum overlap of 80 % was maintained between images to ensure comprehensive coverage and accurate data integration. Although the target surface can be fully reconstructed in 3D without any scale or position information, additional control data (i.e. direct georeferencing) is needed to extract oriented and scaled data (Gao et al., 2017). To ensure accuracy in scale and full georeferencing, ground control points (GCP) were thus distributed widely across the target area.

In the lab, high-resolution UAV images were processed with the PIX4Dmapper software (Fig. 4, step 2). A high-resolution 2D Orthomosaic, a Digital Surface Model (DSM) and a Digital Terrain Model (DTM) were derived at an average ground sampling distance of 5.36 cm pixel^{-1}, ensuring the fidelity and integrity of the spatial data. A normalized digital surface model (nDSM) was also computed by subtracting a DTM from a DSM.

3.2.3. Object-based image analysis (OBIA)

To extract information on boulders from UAV orthoimages and nDSM, we used an OBIA methodology (Ma et al., 2017). This technique consists of an image segmentation by grouping pixels together into vector objects before classifying objects using their properties (e.g., shape, roughness, or spectral properties). OBIA is superior to traditional per-pixel methods because it incorporates spectral information (e.g., colour) and spatial characteristics (e.g., shape, size, geometry, context and pattern), together with textural data and contextual information (e.g., association with neighboring objects) (Fang et al., 2021; Na et al., 2021). By doing so, OBIA mimics the way humans visually interpret the information on aerial photos and satellite images (Blaschke et al., 2014). The advantages of OBIA are that grouped pixels can be assessed together to measure texture and geometry with corresponding summary statistics (Yeomans et al., 2019). OBIA has been widely applied in many fields of geomorphology, such as landslide feature extraction (Martha et al., 2011; Stumpf and Kerle, 2011), geomorphic type classification (d'Oleire-Oltmanns et al., 2013; Drăguţ and Blaschke, 2006) or landform mapping (Feizizadeh et al., 2021) and has increasingly gained attention as geomorphic parameters and their derivatives can be determined more accurately compared to traditional geometric methods (Feizizadeh et al., 2021; Rodriguez-Gonzalez et al., 2010; Chen et al., 2012).

In this study, we used the multiresolution segmentation algorithm from the Trimble eCognition® software (Fig. 4, step 3) to identify boulders in a bottom-up approach where the scale factor in the segmentation – i.e. the scale parameter (SP) – increases with constant increments (Drăguţ et al., 2014). SP values were set to 40 as it provided the best fit and enabled optimal identification of both large and medium-sized boulders. The shape criteria defines to what degree a given shape may influence segmentation (Ulloa-Torrealba et al., 2020) compared to colour; this value was set to 0.3 resulting in a colour weighting of 0.7. Compactness – defined as the ratio of the area of a polygon to the area of a circle with the same perimeter – determines whether the identified objects show a more compact (fringed) or smoother configuration. To ensure the creation of the smoothest outlines for image objects, we assigned compactness a value of 0.8. Among the layers employed for detection (DSM, DTM and orthomosaic raster layers generated with PIX4Dmapper software), the normalized Digital Surface Model (nDSM) was assigned the highest weight to accentuate the significance of height differences and to prioritize accurate delineation of boulders.

3.2.4. Spatial repartition, density, and orientation of detected boulders

The boulder shapefile, generated with the Trimble eCognition® software, was processed in the spatial analysis module of ArcGIS (Fig. 3, step 4). To map the spatial distribution and orientation of boulders from the shape-related attributes, we successively (1) assessed the boulder shapes using the Polynomial Approximation by Exponential Kernel

(PAEK) algorithm to detect overlaps between adjacent polygons; (2) determined the length and orientation of each boulder (longest axis) using the Minimum Bounding Geometry tool which constructs polygons that encompass each individual boulder with a specified minimum bounding geometry. Using boulder density rasters, we (3) identified distinct clusters of high boulder accumulation, and separated these from areas with low boulder density. We then (4) used a kernel density analysis to define a threshold for the reclassification of the raster pixels into 'deposits' (representing individual lobes or ridges) and 'non-deposits.' In a next step, we (5) isolated individual boulders in dense deposits using the centroid of each polygon and (6) finally assumed that boulders oriented perpendicular to the flow indicate high-density conditions and thus are pertinent to our analysis (Karatson et al., 2002; Bertran et al., 1997; Major, 1998; Iverson et al., 2010; Brenna et al., 2020; Kohlbeck et al., 1994; Rust, 1972). Boulders with their longest axes aligned parallel to the flow, typical of lower-density conditions, were excluded as they were not relevant for the present study. After applying a correction for orthogonal boulder rotation during the deposition process by rotating the mean boulder orientation by $-90°$, we deduced the flow direction from the perpendicularly oriented boulders in selected polygons (Fig. 4, step 5). In a final step, we evaluated the accuracy of the OBIA classification with a kappa accuracy assessment.

4. Results

4.1. Dendrogeomorphic reconstruction

A total of 105 trees was sampled in the fluvio-glacial plain below the Grosse Glacier. Of these trees, we had to disregard 31 trees (corresponding to a rejection rate of 30 %) due to the very complex identification of tree-ring boundaries in heavily stressed growth patterns and rot, thus resulting in a total of 74 trees that could be exploited for the dendrogeomorphic reconstruction. The oldest tree selected for analysis reached breast height in ca. 1670 while the youngest tree only attained sampling height in 2004.

The sample size reached 10 trees, i.e. the minimum threshold for the reconstruction of events, in the year 1933 to gradually increase until 1985 ($n = 33$). The number of trees available for analysis increases sharply in the 1990s. Dendrogeomorphic analysis of the increment cores, wedges and cross sections allowed identification and dating of 147 GDs. A vast majority of the GDs were in the form of callus tissues caused by mechanical scarring of stems ($n = 125$, 85 %) and – to a lesser extent – growth suppression induced by crown decapitation or stem burial ($n = 22$, 15 %). Decadal numbers of GDs identified in the tree-ring series remained fairly homogenous between the 1950s and 1990s (14–23 GD. decade^{-1}) but rise to 40 GD. decade^{-1} as a result of the increasing sample size in the early 21st century (Table 1).

Based on the *It* and *GD* thresholds (see red and green dotted lines in Fig. 5), we identify one major event which we interpret to be a GLOF in c. 1958 as well as five smaller events –considered here as torrential floods due to the height of scars, the nature of damage and the spatial distribution of affected trees – in 1979, 1995, 2008, 2009 and 2011 (Fig. 5).

Table 1
Decadal evolution of growth disturbances (GDs) and sample depth between the 1940s and the 2010s.

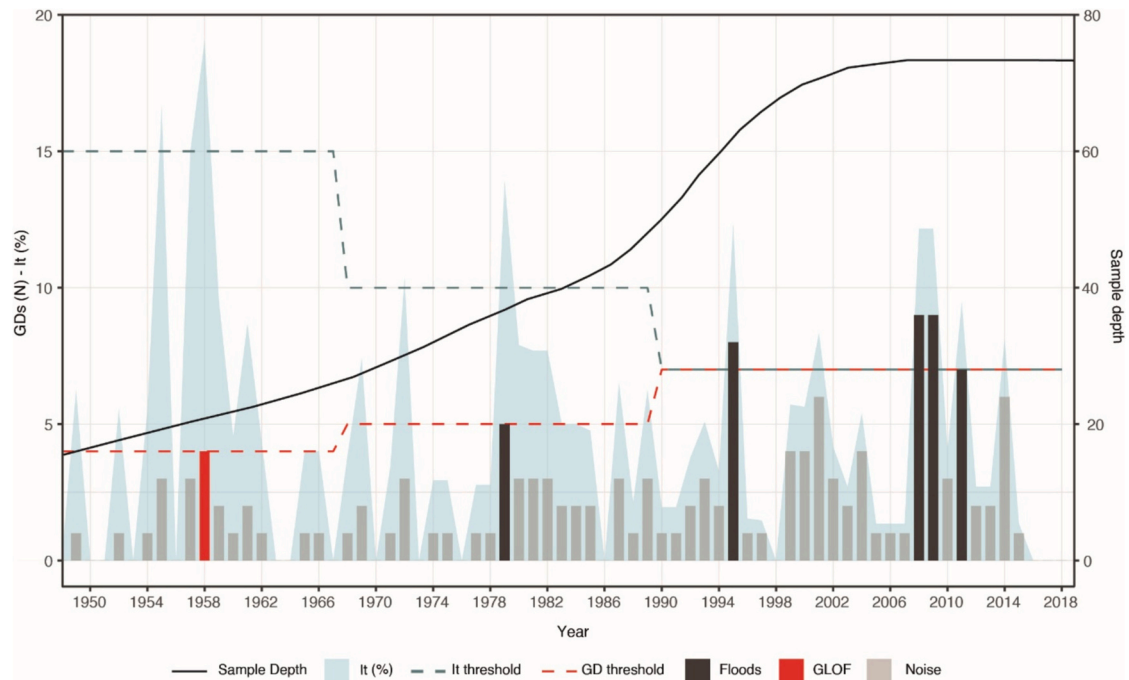| Decades	Σ of GDs	Mean sample depth	Sample depth variation (Δ)
2010	21	74	0
2000	40	73	+3
1990	23	61	+19
1980	22	42	+13
1970	13	33	+15
1960	9	25	+6
1950	14	19	+5
1940	1	13	+5

Fig. 5. Overview of all GD identified in the tree-ring series (grey bars). As the number of samples changes over time (given as a sample depth; black line), we relied on variable index (It) and growth disturbance (GD) thresholds to date past GLOF and flood events. The reconstruction was limited to the period 1933–2019 for which at least 10 trees were available for analyses. A clear peak in the *It* threshold can be found in 1958; damage found in this year stands out clearly and was induced by what is interpreted a GLOF disaster. Five others, yet much smaller episodes with fewer damages can be found in the years 1979, 1995, 2008, 2009 and 2011 and are interpreted here as torrential floods.

4.2. Detection of boulders using object-based image analysis

Boulders were automatically classified from high-resolution UAV images with the Trimble eCognition® software within a ~ 1 km² large area located in the floodplain. These geo-objects were exported as polygons and manually cleaned in ArcGIS software. The cleaning process included the removal of features that were erroneously identified as boulders, the rectification of overlapping polygons as well as the aggregation of adjacent polygons representing a unique boulder, as

illustrated in Figs. 6A, B. Table 2 illustrates the accuracies of image interpretation by assessing our classification (producer accuracy) against the reality on the ground (user accuracy). Results show that 70 % of the boulder and 78.9 % of the deposits present were classified correctly, the mismatches were mainly wrong classifications between these two categories. The overall accuracy as well as the Kappa coefficient of the supervised classification reached satisfactory values (88 and 92.6 %), confirming that our classification to be significantly better than if done randomly.
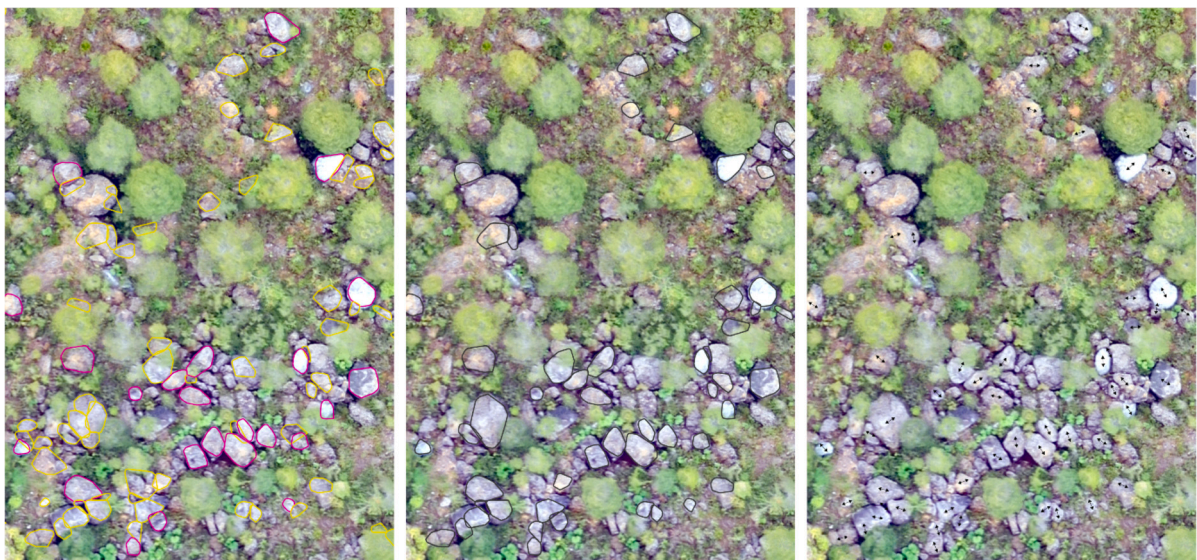

Fig. 6. Illustration of steps 4 and 5 of the object-based image analysis (OBIA): Polygons identified from high-resolution UAV images as boulders and deposits by the automated classification algorithm (eCognition software). Left panel: Pink and yellow polygons represent boulders and deposits, respectively. Middle panel: Boulder polygons were manually rectified (i.e. removal of false positives and false negatives, merging of adjacent polygons) in ArcGIS. Right panel: Determination of boulder orientation was realized with a Polynomial Approximation by Exponential Kernel (PAEK) and minimum bounding geometry algorithms available in ArcGIS.

Table 2
Confusion matrix of the supervised classification analysis of UAV imagery with producer accuracy (false negatives) and user accuracy (false positives).

Classification/ground truth	Boulders	Deposits	Soil	Vegetation	Water	Total	Users accuracy
Boulders	14	4	1	0	1	20	70.00 %
Deposits	5	15	0	0	0	20	75.00 %
Soil	1	0	19	0	0	20	95.00 %
Vegetation	0	0	0	20	0	20	100.00 %
Water	0	0	0	0	20	20	100.00 %
Total	20	19	20	20	21	100	Overall accuracy: 88 %
Producers accuracy	70 %	78.90 %	95.00 %	100.00 %	95.20 %		Kappa Coefficient: 92.6 %

After processing, 1846 boulders with areas ranging from a few to 70 m^2 (Ø 3.8 ± 4.4 m^2) were retained for detailed analyses in the southwestern most part of the fluvio-glacial plain (Fig. 6A). Boulder centroids were used to compute a kernel density map (Fig. 7B) effectively visualizing the concentration patterns of boulders within the study area. This density map, in turn, facilitated the identification of significant deposits and the subsequent quantification of their mean orientation.

This mean orientation, computed as the average direction of boulders within each deposit (Fig. 7B), provides valuable insights into the alignment of the boulder deposits in relation to the potential flow direction (Fig. 7C). After a rotation of −90° applied to the mean boulder orientation, a correction accounting for orthogonal boulder rotation during the deposition process, the resulting map (Fig. 7C) shows a distinct southwest-northeast preferential orientation of the deposits, in line with the direction of an actual secondary river channel.

5. Discussion

In this study, we develop an original approach which aims at reconstructing past (glacial lake outburst) floods (GLOFs) in a region where information on past events is crucially missing. Our study site is located in the Laguna San Rafael National Park, a secluded area where tourism and human activities have been sprawling rapidly over the last decades. In this region, the proximity between human activities and glacial lakes calls for further study as several high-magnitude GLOFs have been reported recently and these occurrences are anticipated to become more frequent and intense in the forthcoming decades (Iribarren

Anacona et al., 2015a; Iribarren Anacona et al., 2015b). More specifically, the Grosse Glacier outlet was chosen after interpreting satellite imagery and historical pictures showing a historical emptying of a lateral lake after 1944–45. To document the assumed event in detail, we developed an original multidisciplinary approach combining remote sensing and tree-ring analyses to precisely delineate the area affected by the GLOF and to date the event.

5.1. Multi-source dating of the post 1944–45 Grosse Glacier GLOF

To reconstruct past GLOF(s) and floods, we sampled *Nothofagus dombeyi*, *N. pumilio*, and *Podocarpus nubigenus* trees showing obvious signs of damage caused by past extreme events. The use of these species is particularly challenging as a result of their complex ring structures. As a result, they have only rarely been considered in dendrogeomorphic studies so far, with the exception of *N. pumilio* which has been the focus of attention among dendrochronologists in southern South America due to its dominance at the tree-line, distinct tree rings and consistent climate–growth relationships (Villalba et al., 1997; Lara et al., 2001; Boninsegna et al., 2009). *Nothofagus* has also been used to reconstruct snow avalanches in Tierra de Fuego (Mundo et al., 2007) or flash floods in the Patagonian Andes (Casteller et al., 2015), but rejection rates of up to two-thirds of the collected samples have been reported due to complex cross-dating between samples and the presence of multiple microrings (Suarez, 2010; Casteller et al., 2015; Stoffel et al., 2019). Likewise, *Podocarpus* has been widely avoided by dendrochronologists due to poorly-defined tree-ring boundaries, ring wedging, and the presence
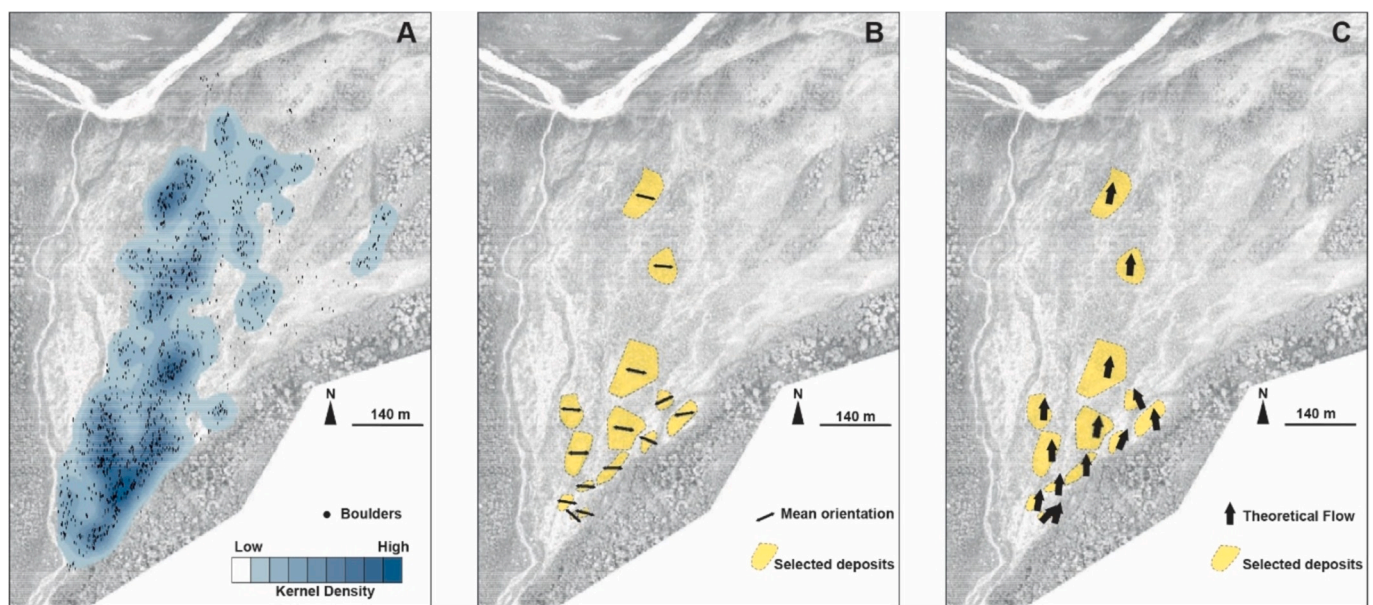

Fig. 7. Detection of boulders in the southwestern part of the fluvio-glacial plain. The Kernel density map (A) highlights areas with high (dark blue) and low (light blue) densities of boulder deposits. Black dots represent the 1846 boulders retained after manual editing in ArcGIS. Mean orientation (double arrow) of boulders (B) in the main deposits (yellow polygons) identified in the fluvio-glacial plain and their respective theoretical direction (C, black arrow) of flows. Boulders were identified using OBIA, deposits were selected following a Kernel Density analysis by keeping only the highest values.

of multiple or missing rings (Rozas et al., 2016; McDougall et al., 2012). Our rejection rate was lower with 30 %, but still substantial. Based on the information contained in the tree-ring records, we reconstruct one GLOF to *c.* 1958 and interpret the spatial and temporal patterns of five smaller torrential events to be the results of floods that occurred between 1979 and 2011.

To define the date of the GLOF more precisely, we conducted interviews with local inhabitants. Although oral history as a research method has some limitations (e.g., recall inaccuracy, selective memories, biases), it has proven to be a useful and credible tool for historical research, especially in places where records do not exist or data collection is not possible (Byers et al., 2020; Sommer and Quinlan, 2018; Yow, 1994). We conducted a unique in-depth and open-ended interview with the only living settler who lived in the area at the time of the GLOF: Juana Guerrero was 87 years old at the time of the interview (2019), and while being confused about her age at the time of the event, she expressed greater confidence in recalling that the GLOF occurred in October 1957. Together with her husband, Juana Guerrero was part of the group of settlers residing in *Puerto Tranquilo* at that time. During that period, they owned cows that grazed in the *Exploradores* valley. She recalled returning to the valley after the event and witnessing numerous cows of various settlers found dead, some stuck up to 6 m high in the trees, in line with scar heights observed during fieldwork and dated to c. 1958 with dendrogeomorphic methods. Likewise, her accounts of where she observed uprooted trees fits with the surfaces where younger recolonize the surfaces with the largest boulders. The accuracy of the testimony can be corroborated further with precipitation records from Puerto Aysen: in fact, the months of September–October 1957 were extremely wet with 17 days of continuous rain and total precipitation of 330 mm. By combining the dendrogeomorphic dating with the eyewitness account and precipitation records from Puerto Aysén, we date the major post-1944–45 GLOF at Grosse Glacier to October 1957.

5.2. Spatial extent and intensity of the 1957 GLOF

While the testimony of Juana Guerrero, the disappearance of the forest cover, and the occurrence of growth disturbances in the tree-ring series collectively indicate the catastrophic nature of the 1957 GLOF, they do not provide insights into its intensity and spatial pattern. Here, we posit that boulder deposits represent a robust signature of past GLOFs (Cook et al., 2018; Huber et al., 2020; Dahlquist and West, 2022) while providing information on their spatial extent and preferential orientation. We thus employed OBIA to locate boulder deposits in the glacio-fluvial plain and to infer the flow direction of the GLOF from boulder orientations. We find that the 1957 GLOF affected both discharge channels with high energy: In the main channel, the frontal moraine remained intact, leading to less solid material load. In contrast, the secondary channel experienced a significant moraine breach introducing a substantial amount of solids and greatly increasing the flow's density. Consequently, we find boulders aligned parallel to the flow direction in the less dense, higher-velocity main channel, while boulders in the more dense, sediment-laden secondary channel would show different patterns and be perpendicularly aligned.

This study therefore also shows that OBIA cannot only be used to quantify the degradation of boulders in complex landslide (Fiolleau et al., 2022), but also to model boulder deposits of GLOFs and to accurately ascertain their orientation across the fluvio-glacial plain. Furthermore, the prevalent southwest-northeast orientation identified in most of the boulder deposits, consistent with the direction of an actual secondary river channel, not only confirms the robustness of the OBIA methodology, but also strongly suggests that a single GLOF occurred in October 1957 and deposited all the boulders or, at least, oriented them in the same direction.

While several GLOF events have been recorded in the region during and before this period, the 1957 event is now the earliest to have been pinned to a given year (Colavitto et al., 2024). The characteristics of the event, originating from an ice-dammed tributary, is remarkably similar to the GLOF that occurred in adjacent Exploradores Glacier in 2018 (Veh et al., 2022), yet has resulted in a much larger and more far-reaching flood.

6. Conclusions

Reconstructing historical GLOFs, especially in remote areas, is an important exercise because detailed case studies of such glacial hazards are rare, which hinders the capacity of glacial hazard practitioners to learn from these events. In this paper, we coupled two approaches, tree-ring and object-based analysis of UAV images, to reconstruct a GLOF that occurred between 1945 and 1974 in the secluded San Rafael National Park in Chilean Patagonia. Despite the difficulties inherent to tree-ring identification and cross-dating the species analyzed in this study, it allowed narrowing down the date of the GLOF and thus provide extensive and valuable information on past GLOF and flood activity in a region that has been largely neglected in terms of hazard and risk assessment. However, estimating the date of occurrence from tree rings alone was not possible. A specific date could only be deduced by adding interviews and the analysis of precipitation records. Similarly, the spatial extent of the GLOF could not be fully inferred from growth disturbances in trees alone, and was thus complemented the study with an object-based analysis of UAV images to map boulder deposits, considered a proxy of high-intensity GLOFs. The spatial patterns of the detected deposits and the flow direction is consistent with the direction of an actual secondary river channel and the morphology of the glacio-fluvial plain, and attest to the high energy of the 1957 GLOF. The results of this study could be used to fine-tune hydraulic models (Ballesteros Cánovas et al., 2011) and improve the accuracy of GLOF hazard and risk prediction further.

CRediT authorship contribution statement

S. Gorsic: Investigation, Formal analysis, Methodology, Visualization, Writing – original draft. **C. Corona:** Conceptualization, Validation, Writing – review & editing. **A. Muñoz-Torrero Manchado:** Methodology, Investigation, Validation, Writing – review & editing. **J. Lopez-Saez:** Visualization. **S. Allen:** Conceptualization, Validation. **J.A. Ballesteros-Cánovas:** Formal analysis, Validation. **A. Dussaillant:** Investigation, Validation, Writing – review & editing. **M. Stoffel:** Conceptualization, Supervision, Funding acquisition, Writing – review & editing.

Declaration of competing interest

The authors declare that they have no known competing financial interests or personal relationships that could have appeared to influence the work reported in this paper.

Acknowledgments

Data availability

Data will be made available on request.

References

Aniya, M., 2013. Holocene glaciations of Hielo Patagˆ|ˆoacute;nico (Patagonia icefield), South America: a brief review. Geochem. J. 47 (2), 97–105. https://doi.org/10.2343/geochemj.1.0171.

Aniya, M., 2017a. Glacier variations of Hielo Patagónico Norte, Chile, over 70 years from 1945 to 2015. Bull. Glaciol. Res. 35, 19–38. https://doi.org/10.5331/bgr.17R01.

Aniya, M., 2017b. Glacier variations of Hielo Patagónico Norte, Chile, over 70 years from 1945 to 2015. Bull. Glacier Res. 35 (0), 19–38. https://doi.org/10.5331/bgr.17R01.

Baker, V.R., 2002. The study of Superfloods. Science 295 (5564), 2379–2380. https://doi.org/10.1126/science.1068448.

Ballesteros Cánovas, J.A., Eguibar, M., Bodoque, J.M., Díez-Herrero, A., Stoffel, M., Gutiérrez-Pérez, I., 2011. Estimating flash flood discharge in an ungauged mountain catchment with 2D hydraulic models and dendrogeomorphic palaeostage indicators. Hydrol. Process. 25 (6), 970–979. https://doi.org/10.1002/hyp.7888.

Ballesteros-Cánovas, J.A., Stoffel, M., Bollschweiler, M., Bodoque, J.M., Díez-Herrero, A., 2010. Flash-flood impacts cause changes in wood anatomy of Alnus glutinosa, Fraxinus angustifolia and Quercus pyrenaica. Tree Physiol. 30 (6), 773–781. https://doi.org/10.1093/treephys/tpq031.

Ballesteros-Cánovas, J.A., Koul, T., Bashir, A., et al., 2020. Recent flood hazards in Kashmir put into context with millennium-long historical and tree-ring records. Sci. Total Environ. 722, 137875. https://doi.org/10.1016/j.scitotenv.2020.137875.

Benito, G., Thorndycraft, V.R., Medialdea, A., Machado, M.J., Sancho, C., Dussaillant, A., 2021. Declining discharge of glacier outburst floods through the Holocene in Central Patagonia. Quat. Sci. Rev. 256, 106810. https://doi.org/10.1016/j.quascirev.2021.106810.

Bertran, P., Hetu, B., Texier, J.P., Steijn, H., 1997. Fabric characteristics of subaerial slope deposits. Sedimentology 44 (1), 1–16. https://doi.org/10.1111/j.1365-3091.1997.tb00421.x.

Blaschke, T., Feizizadeh, B., Holbling, D., 2014. Object-based image analysis and digital terrain analysis for locating landslides in the Urmia Lake Basin. Iran. IEEE J. Sel. Top Appl. Earth Observ. Remote Sens. 7 (12), 4806–4817. https://doi.org/10.1109/JSTARS.2014.2350036.

Bollschweiler, M., Stoffel, M., 2010. Tree rings and debris flows: recent developments, future directions. Prog. Phys. Geogr. 34 (5), 625–645. https://doi.org/10.1177/0309133310370283.

Bollschweiler, M., Stoffel, M., Ehmisch, M., Monbaron, M., 2007. Reconstructing spatio-temporal patterns of debris-flow activity using dendrogeomorphological methods. Geomorphology 87 (4), 337–351. https://doi.org/10.1016/j.geomorph.2006.10.002.

Bollschweiler, M., Stoffel, M., Schneuwly, D., 2008. Dynamics in debris-flow activity on a forested cone — a case study using different dendroecological approaches. Catena 72 (1), 67–78. https://doi.org/10.1016/j.catena.2007.04.004.

Boninsegna, J.A., Argollo, J., Aravena, J.C., et al., 2009. Dendroclimatological reconstructions in South America: a review. Palaeogeogr. Palaeoclimatol. Palaeoecol. 281 (3–4), 210–228. https://doi.org/10.1016/j.palaeo.2009.07.020.

Bräker, O.U., 2002. Measuring and data processing in tree-ring research – a methodological introduction. Dendrochronologia 20 (1–2), 203–216. https://doi.org/10.1078/1125-7865-00017.

Brenna, A., Surian, N., Ghinassi, M., Marchi, L., 2020. Sediment–water flows in mountain streams: recognition and classification based on field evidence. Geomorphology 371, 107413. https://doi.org/10.1016/j.geomorph.2020.107413.

Burton, J.W., Chambers, F.B., Sincavage, R., Cross, M.D., 2022. Analysis of glacial lake outburst flood terrain and sedimentary deposits in Valle Soler. Northern Patagonia Icefield. Phys. Geogr. 43 (3), 333–349. https://doi.org/10.1080/02723646.2020.1839213.

Byers, A.C., Chand, M.B., Lala, J., Shrestha, M., Byers, E.A., Watanabe, T., 2020. Reconstructing the history of glacial Lake outburst floods (GLOF) in the Kanchenjunga conservation area, East Nepal: an interdisciplinary approach. Sustainability 12 (13), 5407. https://doi.org/10.3390/su12135407.

Casteller, A., Stoffel, M., Crespo, S., Villalba, R., Corona, C., Bianchi, E., 2015. Dendrogeomorphic reconstruction of flash floods in the Patagonian Andes. Geomorphology 228, 116–123. https://doi.org/10.1016/j.geomorph.2014.08.022.

Cenderelli, D.A., Wohl, E.E., 2003. Flow hydraulics and geomorphic effects of glacial-lake outburst floods in the Mount Everest region. Nepal. Earth Surf. Process Landforms. 28 (4), 385–407. https://doi.org/10.1002/esp.448.

Chen, G., Hay, G.J., Carvalho, L.M.T., Wulder, M.A., 2012. Object-based change detection. Int. J. Remote Sens. 33 (14), 4434–4457. https://doi.org/10.1080/01431161.2011.648285.

Clague, J., 2000. A review of catastrophic drainage of moraine-dammed lakes in British Columbia. Quat. Sci. Rev. 19 (17–18), 1763–1783. https://doi.org/10.1016/S0277-3791(00)00090-1.

Colavitto, B., Allen, S., Winocur, D., et al., 2024. A glacial lake outburst floods hazard assessment in the Patagonian Andes combining inventory data and case-studies. Sci. Total Environ. 916, 169703. https://doi.org/10.1016/j.scitotenv.2023.169703.

Cook, K.L., Andermann, C., Gimbert, F., Adhikari, B.R., Hovius, N., 2018. Glacial lake outburst floods as drivers of fluvial erosion in the Himalaya. Science 362 (6410), 53–57. https://doi.org/10.1126/science.aat4981.

Corona, C., Lopez Saez, J., Stoffel, M., et al., 2012. How much of the real avalanche activity can be captured with tree rings? An evaluation of classic dendrogeomorphic approaches and comparison with historical archives. Cold Reg. Sci. Technol. 74-75, 31–42. https://doi.org/10.1016/j.coldregions.2012.01.003.

Costa, J.E., 1983. Paleohydraulic reconstruction of flash-flood peaks from boulder deposits in the Colorado front range. Geol. Soc. Am. Bull. 94 (8), 986. https://doi.org/10.1130/0016-7606(1983)94<986:PROFPF>2.0.CO;2.

Coussot, P., Meunier, M., 1996. Recognition, classification and mechanical description of debris flows. Earth Sci. Rev. 40 (3–4), 209–227. https://doi.org/10.1016/0012-8252(95)00065-8.

Dahlquist, M.P., West, A.J., 2022. The imprint of erosion by glacial lake outburst floods in the topography of central Himalayan rivers. Earth Surf. Dyn. 10 (4), 705–722. https://doi.org/10.5194/esurf-10-705-2022.

Davies, B.J., Glasser, N.F., 2012. Accelerating shrinkage of Patagonian glaciers from the little ice age (~AD 1870) to 2011. J. Glaciol. 58 (212), 1063–1084. https://doi.org/10.3189/2012JoG12J026.

d'Oleire-Oltmanns, S., Eisank, C., Dragut, L., Blaschke, T., 2013. An object-based workflow to extract landforms at multiple scales from two distinct data types. IEEE Geosci. Remote Sens. Lett. 10 (4), 947–951. https://doi.org/10.1109/LGRS.2013.2254465.

Drăguţ, L., Blaschke, T., 2006. Automated classification of landform elements using object-based image analysis. Geomorphology 81 (3–4), 330–344. https://doi.org/10.1016/j.geomorph.2006.04.013.

Drăguţ, L., Csillik, O., Eisank, C., Tiede, D., 2014. Automated parameterisation for multi-scale image segmentation on multiple layers. ISPRS J. Photogramm. Remote Sens. 88, 119–127. https://doi.org/10.1016/j.isprsjprs.2013.11.018.

Dubé, S., Filion, L., Hétu, B., 2004. Tree-ring reconstruction of high-magnitude snow avalanches in the northern Gaspé peninsula, Québec, Canada. Arct. Antarct. Alp. Res. 36 (4), 555–564.

Dussaillant, A., Benito, G., Buytaert, W., Carling, P., Meier, C., Espinoza, F., 2010. Repeated glacial-lake outburst floods in Patagonia: an increasing hazard? Nat. Hazards 54 (2), 469–481. https://doi.org/10.1007/s11069-009-9479-8.

Dussaillant, I., Berthier, E., Brun, F., et al., 2019. Two decades of glacier mass loss along the Andes. Nat. Geosci. 12 (10), 802–808. https://doi.org/10.1038/s41561-019-0432-5.

Emmer, A., 2017. Geomorphologically effective floods from moraine-dammed lakes in the cordillera Blanca. Peru. Quat. Sci. Rev. 177, 220–234. https://doi.org/10.1016/j.quascirev.2017.10.028.

Emmer, A., 2023. Vanishing evidence? On the longevity of geomorphic GLOF diagnostic features in the tropical Andes. Geomorphology 422, 108552. https://doi.org/10.1016/j.geomorph.2022.108552.

Emmer, A., Wood, J.L., Cook, S.J., et al., 2022. 160 glacial lake outburst floods (GLOFs) across the tropical Andes since the little ice age. Glob. Planet. Chang. 208, 103722. https://doi.org/10.1016/j.gloplacha.2021.103722.

Fang, X., Li, J., Zhu, Y., et al., 2021. OBIA-based extraction of artificial terrace damages in the loess plateau of China from UAV photogrammetry. IJGI 10 (12), 805. https://doi.org/10.3390/ijgi10120805.

Feizizadeh, B., Kazemi Garajeh, M., Blaschke, T., Lakes, T., 2021. An object based image analysis applied for volcanic and glacial landforms mapping in Sahand Mountain. Iran. CATENA 198, 105073. https://doi.org/10.1016/j.catena.2020.105073.

Fiolleau, S., Jongmans, D., Bièvre, G., Chambon, G., Michel, O., Borgniet, L., 2022. Study of clay degradation in an earthslide combining OBIA and roughness analysis of UAV-based optical images. Earth Surf. Process. Landf. 47 (15), 3465–3480. https://doi.org/10.1002/esp.5468.

Franco-Ramos, O., Stoffel, M., Ballesteros-Cánovas, J.A., 2019. Reconstruction of debris-flow activity in a temperate mountain forest catchment of Central Mexico. J. Mt. Sci. 16 (9), 2096–2109. https://doi.org/10.1007/s11629-019-5496-6.

Gao, M., Xu, X., Klinger, Y., Van Der Woerd, J., Tapponnier, P., 2017. High-resolution mapping based on an unmanned aerial vehicle (UAV) to capture paleoseismic offsets along the Altyn-Tagh fault, China. Sci. Rep. 7 (1), 8281. https://doi.org/10.1038/s41598-017-08119-2.

Harrison, S., Kargel, J.S., Huggel, C., et al., 2018. Climate change and the global pattern of moraine-dammed glacial lake outburst floods. Cryosphere 12 (4), 1195–1209. https://doi.org/10.5194/tc-12-1195-2018.

Hock, R., Rasul, G., Adler, C., et al., 2019. High Mountain Areas. In: *IPCC Special Report on the Ocean and Cryosphere in a Changing Climate*. [H.-O. Pörtner, D.C. Roberts, V. Masson-Delmotte, P. Zhai, M. Tignor, E. Poloczanska, K. Mintenbeck, A. Alegría, M. Nicolai, A. Okem, J. Petzold, B. Rama, N.M. Weyer (eds.)].

Huber, M.L., Lupker, M., Gallen, S.F., Christl, M., Gajurel, A.P., 2020. Timing of exotic, far-traveled boulder emplacement and paleo-outburst flooding in the Central Himalayas. Earth Surf. Dyn. 8 (3), 769–787. https://doi.org/10.5194/esurf-8-769-2020.

IPCC, 2021. *Climate Change 2021: The Physical Science Basis. Contribution of Working Group I to the Sixth Assessment Report of the Intergovernmental Panel on Climate In Press.* [Masson-Delmotte, V., P. Zhai, A. Pirani, S.L. Connors, C. Péan, S. Berger, N. Caud, Y. Chen, L. Goldfarb, M.I. Gomis, M. Huang, K. Leitzell, E. Lonnoy, J.B.R. Matthews, T. K. Maycock, T. Waterfield, O. Yelekçi, R. Yu, and B. Zhou (eds.)]. Change Cambridge University Press. In press.

Iribarren Anacona, P., Mackintosh, A., Norton, K.P., 2015a. Hazardous processes and events from glacier and permafrost areas: lessons from THE Chilean and Argentinean Andes: GLACIER AND PERMAFROST HAZARDS IN THE EXTRATROPICAL ANDES. Earth Surf. Process. Landf. 40 (1), 2–21. https://doi.org/10.1002/esp.3524.

Iribarren Anacona, P., Mackintosh, A., Norton, K., 2015b. Reconstruction of a glacial lake outburst flood (GLOF) in the Engaño Valley, Chilean Patagonia: lessons for GLOF risk management. Sci. Total Environ. 527-528, 1–11. https://doi.org/10.1016/j.scitotenv.2015.04.096.

Iverson, R.M., Logan, M., LaHusen, R.G., Berti, M., 2010. The perfect debris flow? Aggregated results from 28 large-scale experiments. J. Geophys. Res. 115 (F3), F03005. https://doi.org/10.1029/2009JF001514.

Jacquet, J., McCoy, S.W., McGrath, D., et al., 2017. Hydrologic and geomorphic changes resulting from episodic glacial lake outburst floods: Rio Colonia, Patagonia. Chile. Geophys. Res. Lett. 44 (2), 854–864. https://doi.org/10.1002/2016GL071374.

Karatson, D., Sztano, O., Telbisz, T., 2002. Preferred clast orientation in Volcaniclastic mass-flow deposits: application of a new photo-statistical method. J. Sediment. Res. 72 (6), 823–835. https://doi.org/10.1306/040402720823.

Kershaw, J.A., Clague, J.J., Evans, S.G., 2005. Geomorphic and sedimentological signature of a two-phase outburst ?ood from moraine-dammed queen Bess Lake, British Columbia. Canada. Earth Surf Process Landforms 30 (1), 1–25. https://doi.org/10.1002/esp.1122.

Kohlbeck, F., Mojica, J., Scheidegger, A.E., 1994. Clast orientations of the 1985 lahars of the Nevado del Ruiz, Colombia and implications for depositional processes. Sediment. Geol. 88 (3–4), 175–183. https://doi.org/10.1016/0037-0738(94)90059-0.

LaMarche Valmore C., Jr, 1968. *Rates of Slope Degradation as Determined from Botanical Evidence White Mountains California*. U.S. GEOLOGICAL SURVEY PROFESSIONAL PAPER 352–1.

Lambiel, C., Reynard, E., Corboz, P., Bardou, E., Payot, C., Deslarzes, B., 2020. Reconstructing past flood events from geomorphological and historical data. The Giétro outburst flood in 1818. J. Maps 16 (2), 500–511. https://doi.org/10.1080/17445647.2020.1763487.

Lara, A., Aravena, J.C., Villalba, R., Wolodarsky-Franke, A., Luckman, B., Wilson, R., 2001. Dendroclimatology of high-elevation *Nothofagus pumilio* forests at their northern distribution limit in the Central Andes of Chile. Can. J. For. Res. 31 (6), 925–936. https://doi.org/10.1139/cjfr-31-6-925.

Larsson, L., 2013. CooRecorder and Cdendro programs of the CooRecorder/Cdendro package version 7.6. Published online. http://www.cybis.se/forfun/dendro/.

Loriaux, T., Casassa, G., 2013a. Evolution of glacial lakes from the northern Patagonia icefield and terrestrial water storage in a sea-level rise context. Glob. Planet. Chang. 102, 33–40. https://doi.org/10.1016/j.gloplacha.2012.12.012.

Loriaux, T., Casassa, G., 2013b. Evolution of glacial lakes from the northern Patagonia icefield and terrestrial water storage in a sea-level rise context. Glob. Planet. Chang. 102 (March), 33–40. https://doi.org/10.1016/j.gloplacha.2012.12.012.

Ma, L., Li, M., Ma, X., Cheng, L., Du, P., Liu, Y., 2017. A review of supervised object-based land-cover image classification. ISPRS J. Photogramm. Remote Sens. 130, 277–293. https://doi.org/10.1016/j.isprsjprs.2017.06.001.

Major, J.J., 1998. Pebble orientation on large, experimental debris-flow deposits. Sediment. Geol. 117 (3–4), 151–164. https://doi.org/10.1016/S0037-0738(98)00014-1.

Mani, P., Allen, S., Evans, S.G., et al., 2023. Geomorphic process chains in high-mountain regions – A review and classification approach for natural hazards assessment. *Reviews of Geophysics*. Published online September 13. https://doi.org/10.1029/2022RG000791 e2022RG000791.

Mardones, F.M., Aguayo, A.M., Smith, A.E., Ruiz, L.P., 2018. Retroceso glacial reciente en el Campo de Hielo Norte, región de Aysén, Chile: relación con variaciones climáticas. Rev geogr Norte Gd. 69, 121–147. https://doi.org/10.4067/S0718-34022018000100121.

Martha, T.R., Kerle, N., Van Westen, C.J., Jetten, V., Kumar, K.V., 2011. Segment optimization and data-driven thresholding for knowledge-based landslide detection by object-based image analysis. IEEE Trans. Geosci. Remote Sens. 49 (12), 4928–4943. https://doi.org/10.1109/TGRS.2011.2151866.

Masiokas, M., Villalba, R., 2004. Climatic significance of intra-annual bands in the wood of Nothofagus pumilio in southern Patagonia. Trees 18 (6), 696–704. https://doi.org/10.1007/s00468-004-0355-6.

McDougall, K.L., Brookhouse, M.T., Broome, L.S., 2012. Dendroclimatological investigation of mainland Australia's only alpine conifer, Podocarpus lawrencei Hook.F. Dendrochronologia 30 (1), 1–9. https://doi.org/10.1016/j.dendro.2011.01.011.

Morel, M., Piton, G., Kuss, D., Evin, G., Le Bouteiller, C., 2023. Statistical modelling of sediment supply in torrent catchments of the northern French Alps. Landslides and Debris Flows Hazards. https://doi.org/10.5194/egusphere-2022-1494.

Mundo, I.A., Barrera, M.D., Roig, F.A., 2007. Testing the utility of Nothofagus pumilio for dating a snow avalanche in Tierra del Fuego. Argentina. Dendrochronologia 25 (1), 19–28. https://doi.org/10.1016/j.dendro.2007.01.001.

Na, J., Ding, H., Zhao, W., Liu, K., Tang, G., Pfeifer, N., 2021. Object-based large-scale terrain classification combined with segmentation optimization and terrain features: a case study in China. Trans. GIS 25 (6), 2939–2962. https://doi.org/10.1111/tgis.12795.

O'Connor, J.E., Costa, J.E., 1993. Geologic and hydrologic hazards in glacierized basins in North America resulting from 19th and 20th century global warming. Nat. Hazards 8 (2), 121–140. https://doi.org/10.1007/BF00605437.

Piton, G., Fontaine, F., Bellot, H., et al., 2018. Direct field observations of massive bedload and debris-flow depositions in open check dams. Paquier A, Rivière N, eds. *E3S Web Conf*. https://doi.org/10.1051/e3sconf/20184003003, 40:03003.

Piton, G., Goodwin, S.R., Mark, E., Strouth, A., 2022. Debris flows, boulders and constrictions: a simple framework for modeling jamming, and its consequences on outflow. JGR Earth Surf. 127 (5). https://doi.org/10.1029/2021JF006447.

Reardon, B.A., Pederson, G.T., Caruso, C.J., Fagre, D.B., 2008. Spatial reconstructions and comparisons of historic snow avalanche frequency and extent using tree rings in glacier National Park, Montana, U.S.a. Arct. Antarct. Alp. Res. 40 (1), 148–160. https://doi.org/10.1657/1523-0430(06-069)[REARDON]2.0.CO;2.

Rick, B., McGrath, D., McCoy, S.W., Armstrong, W.H., 2023. Unchanged frequency and decreasing magnitude of outbursts from ice-dammed lakes in Alaska. Nat. Commun. 14 (1), 6138. https://doi.org/10.1038/s41467-023-41794-6.

Rivera, A., Benham, T., Casassa, G., Bamber, J., Dowdeswell, J.A., 2007. Ice elevation and areal changes of glaciers from the northern Patagonia icefield. Chile. Global Planet. Change. 59 (1–4), 126–137. https://doi.org/10.1016/j.gloplacha.2006.11.037.

Rodriguez-Gonzalez, A., Fernandez-Turiel, J.L., Perez-Torrado, F.J., Gimeno, D., Aulinas, M., 2010. Geomorphological reconstruction and morphometric modelling applied to past volcanism. Int. J. Earth Sci. (Geol. Rundsch.) 99 (3), 645–660. https://doi.org/10.1007/s00531-008-0413-1.

Rozas, V., Le Quesne, C., Muñoz, A., Puchi, P., 2016. Climate and growth of Podocarpus salignus in Valdivia. Chile. Dendrobiology 76, 3–11. https://doi.org/10.12657/denbio.076.001.

Rudoy, A.N., 2002. Glacier-dammed lakes and geological work of glacial superfloods in the late Pleistocene, southern Siberia. Altai Mountains. Quat. Int. 87 (1), 119–140. https://doi.org/10.1016/S1040-6182(01)00066-0.

Ruiz-Villanueva, V., Allen, S., Arora, M., Goel, N.K., Stoffel, M., 2017. Recent catastrophic landslide lake outburst floods in the Himalayan mountain range. Progress Phys. Geogr. Earth Environ. 41 (1), 3–28. https://doi.org/10.1177/0309133316658614.

Rust, Brian R., 1972. Pebble orientation in fluvial sediments. SEPM JSR. 42. https://doi.org/10.1306/74D7255E-2B21-11D7-8648000102C1865D.

Schneuwly-Bollschweiler, M., Corona, C., Stoffel, M., 2013. How to improve dating quality and reduce noise in tree-ring based debris-flow reconstructions. Quat. Geochronol. 18, 110–118. https://doi.org/10.1016/j.quageo.2013.05.001.

Schraml, K., Oismüller, M., Stoffel, M., Hübl, J., Kaitna, R., 2015. Debris-flow activity in five adjacent gullies in a limestone mountain range. Geochronometria 42 (1). https://doi.org/10.1515/geochr-2015-0007.

Schulman, E., 1956. Dendroclimatic Changes in Semiarid America. University of Arizona.

Shroder, J.F., 1978. Dendrogeomorphological analysis of mass movement on table cliffs plateau. Utah. Quat. Res. 9 (02), 168–185. https://doi.org/10.1016/0033-5894(78)90065-0.

Shugar, D.H., Burr, A., Haritashya, U.K., et al., 2020. Rapid worldwide growth of glacial lakes since 1990. Nat. Clim. Chang. 10 (10), 939–945. https://doi.org/10.1038/s41558-020-0855-4.

Šilhán, K., 2023. Historical activity of debris flows in the medium-high mountains: regional reconstruction using dendrogeomorphic approach. Sci. Total Environ. 856, 159248. https://doi.org/10.1016/j.scitotenv.2022.159248.

Sommer, B.W., Quinlan, M.K., 2018. The Oral History Manual, Third edition. Rowman & Littlefield.

Stoffel, M., Bollschweiler, M., 2008. Tree-ring analysis in natural hazards research - an overview. Nat. Hazards Earth Syst. Sci. 8 (2), 187–202. https://doi.org/10.5194/nhess-8-187-2008.

Stoffel, M., Corona, C., 2014. Dendroecological dating of geomorphic disturbance in trees. Tree-Ring Res. 70 (1), 3–20. https://doi.org/10.3959/1536-1098-70.1.3.

Stoffel, M., Bollschweiler, M., Beniston, M., 2011. Rainfall characteristics for periglacial debris flows in the Swiss Alps: past incidences–potential future evolutions. Clim. Chang. 105 (1–2), 263–280. https://doi.org/10.1007/s10584-011-0036-6.

Stoffel, M., Mendlik, T., Schneuwly-Bollschweiler, M., Gobiet, A., 2014. Possible impacts of climate change on debris-flow activity in the Swiss Alps. Clim. Chang. 122 (1–2), 141–155. https://doi.org/10.1007/s10584-013-0993-z.

Stoffel, M., Ballesteros-Cánovas, J.A., Corona, C., 2017. Šilhán K. Deciphering Dendroecological Fingerprints of Geomorphic Process Activity. In: Amoroso MM, Daniels LD, Baker PJ, Camarero JJ, eds. *Dendroecology*. Vol 231. Springer International Publishing 279–303. https://doi.org/10.1007/978-3-319-61669-8_12.

Stoffel, M., Ballesteros Cánovas, J.A., Luckman, B.H., Casteller, A., Villalba, R., 2019. Tree-ring correlations suggest links between moderate earthquakes and distant rockfalls in the Patagonian cordillera. Sci. Rep. 9 (1), 12112. https://doi.org/10.1038/s41598-019-48530-5.

Stuart-Smith, R.F., Roe, G.H., Li, S., Allen, M.R., 2021. Increased outburst flood hazard from Lake Palcacocha due to human-induced glacier retreat. Nat. Geosci. 14 (2), 85–90. https://doi.org/10.1038/s41561-021-00686-4.

Stumpf, A., Kerle, N., 2011. Object-oriented mapping of landslides using random forests. Remote Sens. Environ. 115 (10), 2564–2577. https://doi.org/10.1016/j.rse.2011.05.013.

Suarez, M.L., 2010. Tree-ring records from Nothofagus dombeyi: a preliminary chronology network in northern Patagonia. Argentina. Dendrochronologia 28 (2), 65–72. https://doi.org/10.1016/j.dendro.2009.11.001.

Taylor, C., Robinson, T.R., Dunning, S., Rachel Carr, J., Westoby, M., 2023. Glacial lake outburst floods threaten millions globally. Nat. Commun. 14 (1), 487. https://doi.org/10.1038/s41467-023-36033-x.

Tichavský, R., Fabiánová, A., Koutroulis, A., Spálovský, V., 2022. Occasional but severe: past debris flows and snow avalanches in the Helmos Mts. (Greece) reconstructed from tree-ring records. Sci. Total Environ. 848, 157759. https://doi.org/10.1016/j.scitotenv.2022.157759.

Ulloa-Torrealba, Y., Stahlmann, R., Wegmann, M., Koellner, T., 2020. Over 150 years of change: object-oriented analysis of historical land cover in the Main River catchment, Bavaria/Germany. Remote Sens. 12 (24), 4048. https://doi.org/10.3390/rs12244048.

Vandekerkhove, E., Bertrand, S., Torrejón, F., Kylander, M.E., Reid, B., Saunders, K.M., 2021. Signature of modern glacial lake outburst floods in fjord sediments (Baker River, southern Chile). Felletti F, ed. Sedimentology 68 (6), 2798–2819. https://doi.org/10.1111/sed.12874.

Veh, G., Lützow, N., Kharlamova, V., Petrakov, D., Hugonnet, R., Korup, O., 2022. Trends, Breaks, and biases in the frequency of reported glacier Lake outburst floods. *Earth's*. Future 10 (3). https://doi.org/10.1029/2021EF002426.

Veh, G., Lützow, N., Tamm, J., et al., 2023. Less extreme and earlier outbursts of ice-dammed lakes since 1900. Nature 614 (7949), 701–707. https://doi.org/10.1038/s41586-022-05642-9.

Villalba, R., Boninsegna, J.A., Veblen, T.T., Schmelter, A., Rubulis, S., 1997. No title found. Clim. Chang. 36 (3/4), 425–454. https://doi.org/10.1023/A:1005366317996.

Willis, M.J., Melkonian, A.K., Pritchard, M.E., Ramage, J.M., 2012. Ice loss rates at the northern Patagonian icefield derived using a decade of satellite remote sensing. Remote Sens. Environ. 117, 184–198. https://doi.org/10.1016/j.rse.2011.09.017.

Wilson, R., Harrison, S., Reynolds, J., et al., 2019. The 2015 Chileno Valley glacial lake outburst flood. Patagonia. Geomorphology 332, 51–65. https://doi.org/10.1016/j.geomorph.2019.01.015.

Yeomans, C.M., Middleton, M., Shail, R.K., Grebby, S., Lusty, P.A.J., 2019. Integrated object-based image analysis for semi-automated geological lineament detection in Southwest England. Comput. Geosci. 123, 137–148. https://doi.org/10.1016/j.cageo.2018.11.005.

Yow, V.R., 1994. Recording Oral History: A Practical Guide for Social Scientists. Sage Publications.

Zaginaev, V., Ballesteros-Cánovas, J.A., Erokhin, S., Matov, E., Petrakov, D., Stoffel, M., 2016. Reconstruction of glacial lake outburst floods in northern Tien Shan: implications for hazard assessment. Geomorphology 269, 75–84. https://doi.org/10.1016/j.geomorph.2016.06.028.

Zaginaev, V., Petrakov, D., Erokhin, S., Meleshko, A., Stoffel, M., Ballesteros-Cánovas, J.A., 2019. Geomorphic control on regional glacier lake outburst flood and debris flow activity over northern Tien Shan. Glob. Planet. Chang. 176, 50–59. https://doi.org/10.1016/j.gloplacha.2019.03.003.